Research Paper ■

Power and Interpretation of Positron Emission Tomography and Magnetic Resonance Imaging of Prostate Cancer in Nude Mouse

Rakesh Sharma, Jose Katz

Abstract. The changes in signal intensity of micro-PET and micro-MRI images of tumors were characterized using histology, »flow cytometry, DNA fragmentation analysis and NMR peaks. This approach was used to assay the chemotherapeutic efficacy based on FDG and intracellular(IC) sodium changes in tumor. A detailed methodology is presented for PC-3 tumor progression. The logic is presented for signal intensities as a result of ion and metabolite changes during tumor cell apoptosis. PC-3 cell lines were compared with DU-145, LNCaP cell lines in culture for the [Na]i and [Ca]i ion sensing dyes, cell death, NMR peaks and apoptosis staining for chemotherapeutic action of different drugs. As a model experiment, PC3 cell lines were injected to propagate prostate tumors in nude mouse. After PC3 tumor imaging, Taxotere VP-16 Etoposide was administered in vivo and imaging was done after 12 hours and 24 hours. Tumors were taken out for immunohistological staining. The micro-PET and micro-MRI images showed increased 18-FDG uptake and sodium signal intensities in tumor. Taxotere induced an increase in IC-Na signal. FDG uptake increased with decreased tumor size. Histological features were analyzed for high tumor risk and decreased tumor viability. Different cell lines showed characteristic fluorescent dye response by different drugs. Sodium NMR method isolated intracellular sodium. Necrosis and fluid were darker on IC-Na images and hyperactive on PET images. Apoptosis rich regions showed characteristic nuclei with S phase DNA histogram, appearing brighter on IC-Na images and mild active on PET images. NMR spectra showed characteristic high phospho-choline peaks. Therefore, the integrated sodium MRI and PET imaging approach offers an in vivo drug monitoring method. The histoimmunological staining of prostate tumor was specific to apoptosis and the NMR peaks were tumor specific.

■ **Infor Med Slov**: 2007; 12(1): 1-14

Authors' institutions: Department of Medicine, Columbia University, New York, NY, USA.

Contact person: Rakesh Sharma, 901 West Jefferson Street, Jeffwood B-7, Tallahassee, FL 32304, USA. email: rs2010@columbia.edu.

Introduction

In recent past, efforts were made for *in vivo* assessment of chemosensitivity assessment of new antineoplastic drugs using molecular biology and cell culture studies. However, the novel molecular imaging approach to design, application and validation of fusion image constructs with incorporation of cell culture studies is good possibility as gold standard to monitor drug effects due to the controlled conditions and easy procedures. The fused magnetic resonance imaging (MRI) and positron emission tomography (PET) imagers predict tumor intracellular processes like glucose uptake, phosphorylcholine. Tumor cell proliferation, apoptosis, malignancy have been reported due to ionic and metabolite changes in cell culture studies in tumors.[1-3] Further, *in vivo* imaging and physiological experiments extract out the tumor intracellular information.[4-7] Our reports showed the potentials of *in vivo* sodium MRI in assessment time-dependent chemosensitivity, tumor pre-malignancy classification and intracellular apoptosis with DNA cycle.[8-10] In present paper, the measurement power is demonstrated to highlight the imaging and cytomorphic methods for the interested readers. These tumor imaging techniques demonstrate the value of ions (by MRI) and physiological weight (by PET) images with cell culture DNA fragmentation, NMR peaks and flow cytometry. In following description, biological associaton of MRI and PET signal origin, ions in tumor, glucose uptake, and tumor cell culture methods are highlighted followed by experimental model of PC3 injected mouse prostate tumor MRI/PET imaging and its histo-immunological correlates.

Increased 18-FDG uptake is a sensitive marker of tumor glycolytic rate and tumor PET characteristic. Empirically, increased 2-deoxy-glucose utilization and increased intracellular sodium appear as a result of apoptosis. We have analyzed this possibility of coincidence of apoptosis, increased intracellular sodium by MRI and glucose utilization by high resolution PET.[11] Further, tissue cells were characterized by DNA fragmentation using florescent flow cytometry.[12,13] This information was exploited for: 1. noninvasive detection of apoptosis using sodium MRI and FDG as target contrast agent for PET; 2. quantitative analysis of apoptosis cell death using proton NMR spectroscopy and DNA fragmentation analysis. Continuous glucose supply via blood is necessary in tumor.[14] Hexokinase in tissue uses glucose as its source of energy in normal conditions via glut 1 and glut 4 surface-transporters while tumors exhibit higher glycolysis. 18-FDG competes with glucose for hexokinase to produce phosphorylated products and trapped [18F] radiolevel generates PET image.[15,16] So, 18-FDG enters in PC3 tumor via same active glucose transporters using sodium/potassium channel in presence of Na^+/K^+ ATPase for its phosphorylation without any further catabolism within glycolytic pathway. As a result, enhanced glucose uptake at the level of Na^+/K^+ ATPase pump showed increased both μPET and μMRI signal intensities. Image signal intensities were result of ion and metabolite changes during tumor cell apoptosis. The metabolically phosphorylated active structures accumulate resulting enhanced intracellular sodium and were used to monitor FDG consumption and intracellular sodium. So, μPET had ability to extract information of blood flow and glucose consumption while μMRI has ability to extract information of glucose or sodium flux across tumor intracellular membrane.[17] These observations were supported by earlier studies using deoxyglucose double tracer technique, autoradiography.[18]

At our lab, hybrid technique was developed using MRI and μPET.[19] In present paper, this approach is used to explore the correlation of sodium image signal intensity, apoptotic cell death, DNA fragmentation analysis and NMR data. The hypothesis was that both increased intracellular sodium and flouro 2-deoxy-glucose utilization in PC-3 tumors were associated with apoptosis as result of accumulation of NMR visible metabolites.

Materials and Methods

PC3 human prostate cancer cells were propagated in nude mice as experimental model of prostate tumor.[9]

In vivo micro-PET/micro-MRI Studies on tumors propagated from human prostate cancer cells

PET imaging of glucose utilization was done in mice 50-75 gms. Animals were anesthetized using isoflurane (1–2% with oxygen flow rate of 1.5 L/min) and adjusted into a house built stereotactic head frame. Tail vein was catheterized for administration of 18-FDG using pediatric polythene tubing PE 10(diameter 0.011 m) and needle 30 G. for 18-FDG 2-3 mCi (from ^{18}F labeled FDG specific activity 500 MBq/ml) injection and dynamic data was acquired for 20 minutes at the midlevel of heart and trunk sequentially moving the imaging table back and forth between two sites to obtain data of accumulation in prostate tumors. For it, PC3 tumor-bearing mice were imaged simultaneously in the prone position in the μPET scanner (Concord Microsystems, Knoxville, TN). The data included spillover of the radioactivity accumulated in the adjoining muscles around the tumor. To minimize it, radioactivity curve was recorded to have steady state of radioactivity distribution and sequential scanning over tumor area was done using 1.25 mm slice each step. Data were corrected for uniformity, sensitivity, and attenuation and images were reconstructed using Hanning filtered convolution backprojection with cut off value of 1.0. μPET data were corrected for acquisition time, decay and injected dose. PET images were fused with transaxial MR images and using MEDEX software drew volumetric region of interest.[20] Average radioactivity and intracellular sodium concentration per voxel was calculated in different tumor regions.

Proton, ^{23}Na SQ and ^{23}Na TQ images and line profiles were acquired at baseline and following *in vivo* injection of chemotherapy. Acquisition time was 65 min for TQ line profile and 65 min for a full TQ image. Gradient-echo images (3D; 24 slice) were acquired on a high field (4.23 Tesla) whole body MRI (Hatch Center) employing a small quadrature birdcage radiofrequency coil (50 mm ID, Morris) and high strength gradient insert coil (30 mT/m, Bruker, G-33). Following control tumor image acquisition, Taxotere (40 mg/kg; n=5) or VP-16 Etoposide (1.2 mg/kg; n=7) was administered intra-venous.

Fusion of micro-PET/micro-MRI images and postprocessing

For standardization, projection data were acquired for two axial positions with an overlap of ten planes. For both positions, emission and transmission data were acquired over 20 and 10 min, respectively.[20] To combine the high sensitivity of the 3D measurement with the advantages of iterative 2D image reconstruction, transmission-and scatter-corrected emission sinograms were sorted into 2D sinograms using the Fourier rebinning (FORE) algorithm.[19,20] The attenuation and emission images were iteratively reconstructed by means of a high-over relaxation single-projection (HOSP) algorithm with optimized overrelaxation parameters on a Sun Workstation (Ultra Sparc-II/2, Sun, Mountain View, Calif.). Using this ultra-fast algorithm, six iteration steps were sufficient to accurately quantify regional activity and attenuation values.[20] The discretization of the image matrix was 128×128 pixels with a size of 3.9×3.9 mm^2. After reconstruction, images from two adjacent sections with a thickness of 2.46 mm each were added, in order to improve image quality and to enable a correlation with the corresponding MR maps, which were acquired with a larger nominal slice thickness of 5 mm. After correction for radioactive decay (Tm=2; 109:7 min), the FDG uptake was expressed as standardized uptake value (SUV) = tissue concentration (kBq/ml) / injected dose (kBq) per body weight (g).

To improve the anatomical localization of tissue regions with an abnormal FDG uptake, the

reconstructed SUV maps were superimposed (using color shading) onto the corresponding transmission images (in black and white).

Image and data analysis

For a quantitative analysis, regions of interest (ROIs) were placed over the suspicious tumor masses visualized on the images from one modality, and also on the corresponding image regions from the other modality. The superposition of emission and transmission PET scans allows an accurate anatomical localization of tissue regions on the emission scans. Suspected areas of abnormal Gd-DTPA and/or FDG uptake in the tumor were recorded. The results obtained with both imaging modalities were compared with one another, as well as with the results of the histopathological examination. The chemosensitivity effect on 3D FLASH images and color-coded pharmacokinetic parameter maps was analyzed for irregular or stellate shape, a distortion of tissue architecture, and/or an irregular or rim-like enhancement in support of malignancy. On the color-coded pharmacokinetic parameter maps, ROIs were placed to assess the shape of the entire signal ± time course. A rapid rise followed by a plateau or a washout phase or peak enhancement was considered to be suggestive of cancer. A slow signal rise indicated benign nature. Quantitative parameters of morphologic features were empirical scores to yield a sensitivity 86% and specificity 85%.[19] Due to the limited spatial resolution of the PET scans, mean SUVs were evaluated from ROIs placed over tissue regions with a suspicious FDG uptake (70% isocontour curve). To correct the underestimation of activity concentrations in small tissue regions, the SUVs were divided by recovery coefficients.[24] The focal areas of circumscribed elevated tracer uptake with an SUV > 2.5 were classified as carcinomas. The SUV exceeded the SUV in a contralateral reference region by a factor of 10 for cancer. The enhanced sodium and/or FDG uptake, the correlation between MR signal intensity and the SUV was tested at a significance level of $p=0.05$, by calculating Spearman's rank correlation coefficient rS.[20] Statistical analysis was performed using the SPSS software package (version 6.1.2, SPSS, Chicago, Ill).

In vitro tumor cell culture studies

The human prostate cell lines were used in culture studies and tumor propagation in mice. In PC3 cell culture experiments, ratiometric ion sensing fluorescent dyes (Molecular Probes) were used for the Taxotere (10 nM).[21]

Sodium green pilot study was done using sodium green as molecular probe using standard Fluorescein excitation/ emission wavelengths. Forward scattering was used to normalize for loading, or alternatively Na^+ insensitive fluorescent dyes with similar loading behavior e.g. calcein/AM as molecular probe as a control to identify loading variants.[22]

In vitro Na NMR Spectroscopy Studies on superfused human PCa cells

PC 3 cells were embedded in agarose beads, which were perfused in an NMR tube. ^{31}P and ^{23}Na TQ spectra of perfused PC 3 cell loaded agarose beads were first acquired at baseline. Subsequently, 100-nM/L Taxotere was added and ^{31}P-^{23}Na TQ spectra were again acquired at various times.[23]

Prior to recovery from the final imaging session, tumors were recovered from animals and sectioned for following *(a) Histology*: flash frozen for histology and immunohistochemistry- routine H&E, single-strand DNA (ss-DNA) monoclonal antibody (Chemicon International, CA), DNA cycle analysis; *(b) Cells cultured and fixed flow cytometry*: sections were treated with collagenase, and cultured or fixed for flow cytometry study. Flow cytometric data of fixed cells dissociated from treated tumors were compared with those directly from commercial stocks and treated in culture. This comparison assessed adequacy of *in vivo* drug levels. Cells from the dissociated tumor were put into culture (instead of being fixed). These cells were grown overnight and then

subjected to MTT analysis, flow cytometry, DNA fragmentation.[24]

Correlation of histological features with intracellular sodium MRI image signal intensity

The correlation analysis was performed for each tumor slice and data was compiled in a three-dimensional array after stereotactic match of image with histology section (see Figure 1). A method was developed to match and correlate histology and sodium MR images at different regions in the tissue to test null hypothesis. The hypothesis was that altered sodium signal intensities do correlate with immunohistology and cytopathologic parameters. Step-down multivariate statistical analysis was performed to determine the pertinent immunohistological and pathologic parameters, which correlate with the MRI signal for intracellular sodium (IC-Na).

Results

Prostate tumors were 1-2.5 mm rounded shaped propagated with both PC3 and DU145 cell lines.

In vivo micro-PET/micro-MRI signal intensity and histology correlates in tumors propagated from human prostate cancer PC3 cells

18-Fluoro-deoxy-glucose (FDG) uptake, apoptosis and IC-Na changes were seen within hours of exposure of cancer cells to antineoplastic drug as shown in Figure 1. Postmortem analysis (histology; *in situ* TUNEL assay, n=10 tumors) showed cancer cells had decreased mitotic figures in treated vs untreated tumors (2.2 vs 8.6/field; $p<0.0001$). Mitotic suppression correlated with increased IR image intensity for individual tumors ($p<0.02$) as shown in Table 1. Central necrosis and fluid were dark on IR image, while enhanced image intensity correlated with active apoptosis, where cells, as shown, presumably have elevated $[Na]_i$. Co-registered histological sections (Feulgen labeling to nuclear DNA content by CAS 200) showed DNA content of cell nuclei, which varied according to their cell cycle (G1/S-G2/M) and distinct S, M histograms shown in Figure 1 at bottom. FDG uptake was also varied for radioactivity injected, tumor metabolism and drug dose. However, we used optimum dose 125 μCi for 90 minutes that generated matched PET images with MRI images. At this dose, FDG uptake reached at peak in tumor after 40-45 minutes that remained almost constant whole rest of period during imaging (see Figure 1 in top row).

Features indicative of drug effect and neoplasia could be identified, i.e., mitosis, apoptosis rim and nuclear s-DNA contents at different locations of prostate tumor. Pentachrome staining offered 'IC/EC ratio' as marker of viable cells (60-70% with high mitotic index) and apoptotic cells at risk or dying cells (>70% with high apoptotic index). These post-Taxotere injected tumor tissues (in 80% sections) exhibited decreased tumor viability 15 times (mitotic figures ~240 per mm^2 to ~9 per mm^2) and confirmed by lower proliferation index (PI), compared with control tissues. Cell cycle of tumor cells showed reduced diploidy or aneuploidy in dividing tumor cells undergoing cell division in >75% tumor tissues after Taxotere treatment.

Taxotere-treated animals showed single cell necrosis after 12 hours and followed active apoptosis after 24 hours, due to possible chemosensitive effect.

Important features in co-registered IC-Na, μPET hypermetabolic and monoclonal antibody (ss-DNA) sensitive regions were identified which were compared (% difference > 6%) (see panels at bottom row in Figure 1). Parameters like cell cycle distribution and endlabelled DNA strand breaks (both from fluorescent-stained DNA) were sufficiently stable during the approximately 2 hrs required to disperse and fix the cells. Necrosis and fluid were darker on IC-Na images and hyperactive on PET images while apoptosis rich regions showed characteristic nuclei with S phase DNA histogram, appearing brighter on IC-Na images and mild active on PET images.

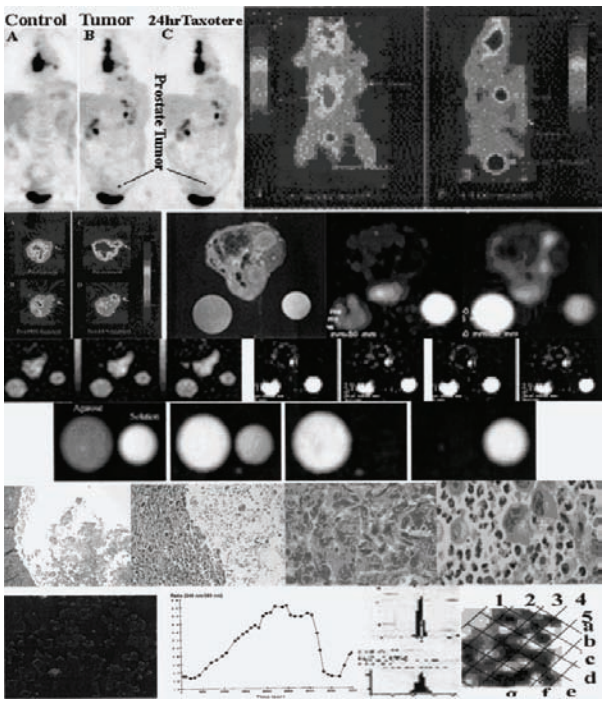

Figure 1 Mouse prostate tumor excitation μPET images before (gray) and after segmentation images are shown as coronal images (panels on top row). Each image set is shown before (left panel) and after drug treatment (right panel) and their counterpart transaxial images (left panels in second row) with their counterpart MRI images (proton T1 image in leftmost panel) and SQ sodium image before (middle gray image) and after Taxotere treatment (right panel). A representative micro-MRI sodium SQ image slice series is shown at various levels (left three panels in third row) for comparison with sodium IR image series (right three panels). In fourth row, sodium phantom tubes are shown as large tube filled with free Na or NaCl and small tube filled with bound sodium with agarose for intracellular sodium solutions. By changing inversion time values (TI), extracellular sodium may be suppressed (rightmost panel). The fifth row displays cyst with extracellular space, necrosis, aneuploidy; the sixth row shows apoptosis (by flow cytometry), μPET biotransformation, M/S neoplasia histograms and pixel matched DNA cycle map.

MRI-PET image registration

The tumor areas in five mouse prostate tumor tissues were sampled by subsampling steps. By manual reorientation using pseudo markers, the tumor regions on MRI and PET images were prealigned. The volume 'trimming' removed the extra image points not common to both PET and MRI imaging data sets as shown in Figure 2. The rigid geometric transformation by AIR and MI algorithms generated 'convergence optimization' of common data points of tumor visible on both MRI and PET images. The singular value decomposition (SVD) algorithm estimated the registration errors up to 10% and generated "perfect" registration transformation matrix by applying transformation to a set of points spaced in and around the mouse tumor. These set of points in registration transformation matrix visualized tumor pixels after retransformation with the inverse of the transformation matrix. The mean Euclidean distance between these final points in fused coregistered images and the maximum distance between these points measured up to ±10% accuracy as "functional performance" of the SVD algorithm.

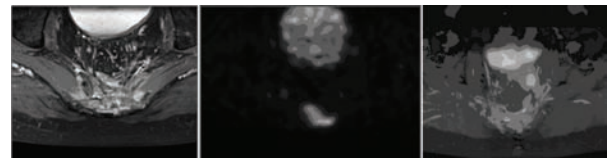

Figure 2 Using ultra-fast algorithm, six iteration steps accurately quantify regional activity and attenuation values. The discretization of the image matrix was 128×128 pixels with a size of 3.9×3.9 mm2. After reconstruction, PET images (in the middle panel) from two adjacent sections with a thickness of 2.46 mm each were added, in order to improve image quality and to enable a correlation with the corresponding MR maps (left panel), which are acquired with a larger nominal slice thickness of 5 mm. The technique fuses both image types to construct fusion image (rightmost panel).

In vitro NMR Spectroscopy Studies on superfused human PCa cells

Although no significant changes in the phosphorous spectra were observed even after 2.5 hours of chemotherapy. NMR spectra showed characteristic high phospho-choline peaks. A significant increase of 24% was already apparent in the ^{23}Na TQ spectra amplitude at 1.5 hours after

chemotherapy. It was indicative of the fact that there was a $[Na]_i$ increase in the tumor cells. Following 3.5 hours of Taxotere, an even further increase of the TQ amplitude was observed (31% compared to baseline; Figure 3).

Na MQF spectroscopy showed that the agarose beads are permeable to Na based on the transitional TQ signal generation from agarose beads mixed with a Na containing solution. TQ spectrum was acquired for agarose beads employed for the cell perfusion system at various creation times. These spectra showed that the transverse relaxation times of agarose beads were much larger than that for the tumor cell pellets. Optimum creation time (time necessary to maximize the TQ signal) was about 3.2 msec for cells and about 31 msec for the agarose beads.

^{31}P and ^{23}Na TQ spectra of perfused PC 3 cell loaded agarose beads were acquired at baseline. Subsequently, 100-nM/L Taxotere was added and ^{31}P-^{23}Na TQ spectra were again acquired at various times as shown in Figure 3. Changes in the phosphorous spectra were observed after 2.5 hours of chemotherapy. ^{23}Na TQ spectral changes were observed at 1.5- 3.5 hours of Taxotere.

SQ and TQ sodium image intensity variants

SQ and TQ Images of a large tumor are shown in Figure 4. Sodium signal intensity was higher in tumor compared to normal tissue in the Na images. However, there was a higher contrast between tumor and normal tissue in the TQ image compared to the SQ image. It was due to higher sodium sensitivity to TQ NMR. Images are shown for *in vivo* injection of 1 mg of Taxotere in the femoral vein. SQ line profiles did not significantly vary. There was a substantial increase in the TQ line profiles following chemotherapy shown by NMR spectroscopy. These results indicate that $[Na]_i$ increased due to chemotherapy based on non-NMR methods and TQ imaging but not by SQ imaging. TQ images were acquired here by use of a standard copper coil. Using high temperature super conducting coil, increased signal-to-noise ratio in Na imaging by a factor of 10 and decreased imaging time by, a factor of 100.

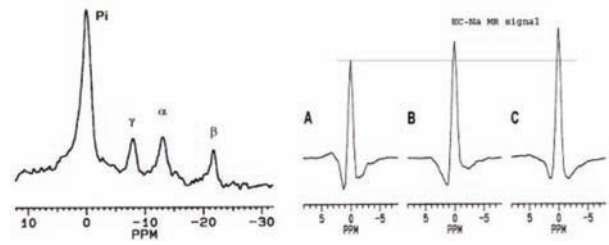

Figure 3 ^{31}P spectrum (left panel) was acquired from perfused PC3 cells in agarose beads before chemotherapy. No significant change in the spectrum was observed following 2.5 hours of drug exposure (100 nM of Taxotere). The alpha-, beta-, and gama-ATP peaks are well resolved and the Pi peak is due to ^{31}P in the perfusate. Exp. cond.: pulse sequence=single Rf pulse followed by signal detection, Rf flip angle=70°, repetition time=1 sec, and total acquisition time=1 hour. ^{23}Na TQ spectra (right panel) acquired from perfused PC3 cells in agarose beads before (**A**), 1.5 hours (**B**), and 3.5 hours (**C**) after chemotherapy (100 nM of Taxotere). Exp. cond.: pulse sequence=with the Rf phases cycled for TQF, repetition time=0.2 sec, creation time=3.2 ms, evolution time=0.1 ms, and total acquisition time=20 min.

Monitoring of therapeutic response by tumor signal intensity in IR Na image

The technical use of SQ and IR sodium images were evaluated visually for diagnostic accuracy and its value in drug therapeutic monitoring. Taxotere enhanced intracellular sodium up to a certain peak time and later the effect was reversed (Table 1). On histology sections from same tumor regions, mitotic figures were inversely correlated.

Selective acquisition of intracellular ^{23}Na by use of inversion recovery (IR)

To visualize PC3 induced tumor morphological details, both SQ and IR sequences were applied. The effects of varying inversion time (TI) and echo time (TE) were indicative of the intracellular sodium signal dependence on these values. The tumors were comparable on sodium images with phantom images as shown in Figure 1.

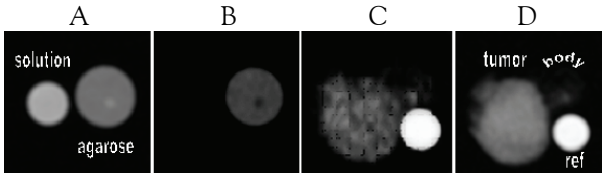

Figure 4 Selective acquisition of intracellular ^{23}Na by use of inversion recovery (IR). Regular SQ (image A) and IR (image B) spin echo images of a phantom. The phantom consists of a left tube filled with 1 M NaCl solution (to simulate EC Na) and a right tube filled with 1 M NaCl in 4% agarose (to simulate IC Na). The images A and B are normalized. The magnetic field was 4.0 T and the inversion delay (τ_1) was 31 ms. T_R=0.2 s and echo time (TE)=8.4 ms. Regular SQ (image C) and IR (image D) gradient echo images of the nude mouse with a PC3 tumor. The image D was enhanced to show the internal structure of the tumor. The reference phantom was filled with 400 mM NaCl in 4% agarose. The magnetic field was 4.0 T and the inversion delay (τ_1) was 31 ms. T_R=0.2 s and T_E=3.2 ms. The imaging time for images C and D was 8 and 32 min, respectively.

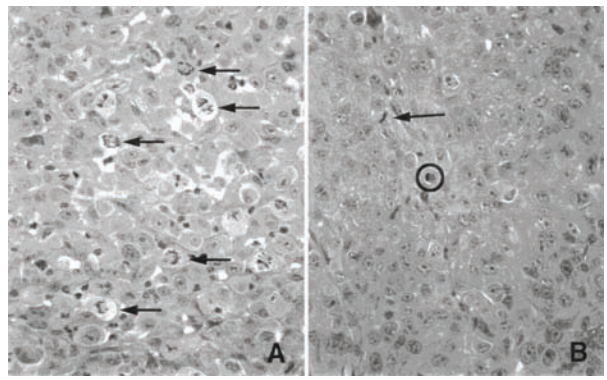

Figure 5 A representative PC3 mouse tumor region rich with apoptosis is shown under high power field of optical microscopy to show beaded nuclei in tumor (see the circle) and membrane blebbing (see the arrows). The comparison of tumor apoptosis rich regions is represented before (left panel) and after Taxotere treatment (right panel).

Table 1 Quantitative evaluation of PC3 prostate tumor shows comparison of MRI-PET imaging by sodium MRI and SUV with cytomorphic indices to interpret the power of signal intensities before and after 24 hours Taxotere treatment in mouse tumor to represent chemosensitivity.

Pre-drug treated[@] and post-drug treated[#] tumor features	Sodium MRI intensity	SUV (kBq/ml)	Histology (in HPF)	A.I. (KI-67)	P.I. (in HPF)	S-DNA (histogram)	ss-DNA mAb (density units)
Tumor area (mm^2;n=16)[@]	4.46±0.3	-	4.4±0.2	-	-	3.2±0.2	4.0±0.2
Tumor area (mm^2;n=3)[#]	4.55±0.2	-	4.32±0.3	-	-	3.0±0.3	4.2±0.3
IC/EC space[@]	65-70	-	65-76	-	-	-	-
IC/EC space[#]	85-95	-	60-70	-	-	-	-
Necrosis* (squares)[@]	gray	85	46±22	-	270	M-DNA	-
Necrosis* (squares)[#]	bright	62	50±21	-	120	M-DNA	-
Viable** (squares)[@]	dark	34	62±21	-	-	-	-
Viable** (squares)[#]	dark	22	74±11	-	-	-	-
Apoptosis*** (nuclei)[@]	bright	45	45±12	150	-	S-DNA	155±15
Apoptosis*** (nuclei)[#]	bright	35	30±13	110	-	M or S-DNA	130±20
Cyst**** (size in μm)[@]	gray	115	125±29	-	-	-	-
Cyst**** (size in μm)[#]	gray	100	82±22	-	-	-	-

Pre-drug treated tumor ([@]) and post-treated tumor ([#]) by sodium MRI image intensity and histology. By using eyepiece-micrometer square counter, necrosis*(<25% cells in micrometer square), viable cells** (<60% cells in micrometer square) and apoptosis*** (20-40 apoptotic nuclei in HPF) and cyst space****(< 100 μm) per HPF were premalignant histology characteristics. IC/EC space (% space in HPF), necrosis, viable cells are shown as number of micrometer squares with <25% necrosis area in HPF by histology. Apoptotic index (A.I.) and proliferation index (P.I.) are shown as average number of apoptotic nuclei per HPF and number of mitotic figures per HPF. S-DNA histogram area was measured by CAS 200 system in arbitrary units. Single strand-DNA mAb area was measured in digital images by Optimas 6.5 and ss-DNA mAb density was measured in arbitrary units of photomultiplier scanner.

Differentiation between apoptosis and necrosis

The distinction was based on the assumption that apoptotic cells may expel propidium iodide even during the period of DNA fragmentation due to advanced stage of deterioration. On the other hand, necrotic cells lose membrane integrity early. Thus a two fluorescent DNA stains with different spectral properties were applied at different times, propidium iodide (PI) first, and subsequently Hoescht 342 was applied after a delay so that apoptotic cells progress to their advanced stages as shown in Figure 5.

Discussion

The present study represented a reasonably reliable interpretation of rapid μPET and sodium MRI *in vivo* monitoring chemotherapeutic response and further investigation on prostate cancer cell lines and tumor physiology in presence of anticancer drugs. However, the efforts to explore the potentials of microimages are still in progress and appeal for better understanding of tumor molecular correlates.

Based upon various reports on animal experimental models used for chemotherapy and cancer prevention studies, μPET, sodium MRI and tumor characterization appears to be particularly relevant to our studies on tumor development, progression of prostate cancer, and treatment efficacy after anticancer drug administration in mouse model simulating human prostate cancer. *In vivo* high-resolution quantitative imaging techniques may provide longitudinal information of multiple simultaneous intracellular processes in tumor initial development. In our earlier report, PC-3 induced prostate tumors in mouse visualized by μPET images showed enhanced glucose uptake tumor activity.[25] We showed enhanced intracellular sodium signal intensity on MR sodium weighted benign and malignant tumor images following Taxotere administration. These MRI signals were correlated for neoplasia and histological characteristics of the excised tumors.[8] However, ionic alterations during malignant transformation, apoptosis, necrosis, and progression through cell cycle have been widely known fact.[26-28] It may be possible that antineoplastic agents affect intracellular ions.[29-32] μPET and sodium MRI imaging with tumor histological and immunostaining characterization of prostate cancer of animals is likely to answer the internal tumor environment better. However, the present study will serve as guideline for both the μPET, sodium MR imaging and tumor immunological and histological correlates.

In the present study, from the MRI standpoint, application of new technique offers intracellular sodium imaging of tumor. From μPET standpoint, the tumor kinetics of F-18 FDG uptake is standardized in prostate tumor. The present study highlighted the integrated μPET-MRI technique reliability and its power of cell resolution up to some extent. These preliminary studies of enhancement in intracellular sodium, glucose utilization and tumor NMR visible metabolites clearly demonstrate them as a consequence of apoptosis or programmed tumor cell death.

Na-NMR spectroscopy studies in cell cultures determined the transverse and longitudinal relaxation times of the sodium nuclei to systematically assess changes in $[Na]_i$ by means of a noninvasive technique. ^{23}Na NMR spectroscopy studies of cell system appeared as an important intermediate for the ultimate clinical implementation.[33] ^{31}P-NMR spectral peaks of enhanced phosphorylcholine/choline were product of choline kinase due to choline trap and phosphorylation in tumor cells.[34-35] [18F]fluoroethylcholine has been reported PET contrast agent based on ^{31}P NMR spectroscopy data.[36]

Standard NMR spectra were acquired for each mice simultaneous with sodium SQ and MQ images at 12 months after cancer cell injections at which point tumors became large enough.[37] The protocols were constrained by the maximum duration of imaging sessions not exceeding beyond

2-hour period of anesthetization during which animals were motionless could readily be attained.

In the present study, dose dependence and time course were studied using *in vivo* Na-NMR studies on commonly known prostate cell lines and tumor cells for the action of antineoplastic drugs. This plan facilitated comparison of tumor image intensity with normal cells and subcutaneous tumor cells propagated from different cell lines to establish rapid assay showing the effect of chemotherapeutic action. Further, the chemotherapeutic action was characterized by postmortem cell culture and ionic alterations.[38]

Premalignant and malignant lesions in mice injected with PC-3 at 50 days of age had various similarities such as biological, morphological, and molecular properties with many characteristics observed in the human disease process that closely mimic human prostate cancer. Although there are several distinct dissimilarities and there are several advantages of this mice model also. The mouse model may be ideally employed to represent progression of human prostate cancer.

The results of our study are consistent with earlier reports of elevated uptake of FDG, intracellular NaI in both benign and malignant breast tumors, neoplastic, well-differentiated and poorly differentiated tumors than in their normal cellular counterparts.[39-40] The logic of these reports was based on the fact that tumor radio-pharmacodynamics and ionic alterations are important events in malignant transformation, apoptosis and necrosis, and progression through the cell cycle. It is not surprising that successful administration of antineoplastic agents may affect intracellular ions also, specifically $[Na]_i$ and $[Ca]_i$. However, the effect of neoplastic agents on F-18 FDG dynamics in prostate tumor is not known. Antineoplastics can change cell cycle distribution often lead to apoptosis, and both changes in cell cycle phase and apoptosis alter $[Na]_i$. *In vivo* injection doses for all drugs used for mice were comparable to human clinical doses in present study. Furthermore, injected doses were at the high end of the maximum tolerable dose (MTD) range for mouse.

Based on our *in vivo* and prostate tissue studies, and *in vitro* literature reports on increased intracellular sodium following chemotherapy appeared indicative of increased $[Na]_i$ at subphysiological level possibly associated with glucose uptake mechanism at the level of inner membrane.[41]

We have, however, considered several alternate explanations for change in intracellular T1 (or change in extracellular T1) and higher 18-Fluoro 2-deoxy glucose uptake. Tumor tissue, where there is a high density of sodium channels and Na/K ATPase pump sites, there seems no evidence of bulk changes in extracellular sodium [Na]i, beyond the unstirred layers around channel pores. It may be speculated that drug induced processes could alter production of metalloproteases, affecting the density of extracellular Na binding sites and result with reduced IC T1 (or increased EC T1) could also contribute to increased glucose uptake across the membrane at the cost of high Na^+/K^+ ATPase pump activity. This explanation answers both increased sodium image intensity and higher FDG uptake. Obviously large changes in [Na]i by themselves could alter IC T1. However, during the tumor hypoxia or ouabain induced increase in [Na]i and IC T1 values were reported independent. [42]

Long-term goals of this enhanced intracellular sodium facilitated glucose uptake in tumor concept are confounded by various issues, which are tumor specificity, tissue cell membrane characteristics, subcellular metabolites, compartmentalization and membrane damage at molecular level. These factors have been studied in present study to answer ionic, metabolites and membrane changes by using sodium MRI, μPET, NMR, fluorescent flow cytometry and DNA fragmentation analysis. It was assumed that different exchange rates of sodium with different T1 values and different FDG uptake rates in different cellular domains reflect the manifestations of inner membrane breaks and

alterations of DNA fragments. However, this presumption needs to be carefully investigated during and after drug treatment.

The correlation between apoptosis and sodium MRI or deoxy-glucose uptake PET image intensity is apparent in comparing the histology, and images.[43,44] Tumors with significant fluid spaces or large centers with cellular debris had dark centers on the sodium images. In present study, the tumor showed low SQ signal and tumor had a larger non-viable center with significant fluid. Other tumors with brighter rims showed sizable different cell stages of apoptosis. Tumors with bright centers had back-to-back apoptosis extending into the central region with minimal non-viable tissue. Although time-dependent study of the histological parameters could not be done due to experimental restrictions, the results were suggestive of brighter apoptosis-rich regions and/or early apoptotic processes in the surviving rim. However, ploidy analysis and H & E stained slices also support these observations.[45] Stereo-micrometric co-registered divisions on digital histology and IR images further enhanced the power to analyze the cellular details at different locations in the tumors as shown in Figure 1.

It is noteworthy that the single strand DNA monoclonal based method enhanced the power of detection for different stages of apoptosis in tumor that was consistent with other reports.[8] Spatial resolution of the image (~ 1 mm within each slice) was affected by the enhanced signal intensity. It could be worsened from a spatial broadening of the apoptotic-localized region or an increased density of apoptotic cells including cells in early apoptotic stages, or both. However, other histoimmunoassay methods may speculate it better such as caspase based methods for different apoptosis staging in tumors.

Apoptosis is a dynamic process, which ends with complete fragmentation and loss of cell nuclei and most of the other cellular macromolecules. Hence, the absence of a weighted IC Na MR signal intensity in late apoptosis can be explained by the loss of polyanions, as the IC space equilibrates its chemical composition with the subcellular fluid. This prediction was consistent with previous finding in prostate tumor that the average IR-sodium intensity increase was smaller at 48 hours than at 24 hours.[9]

The pixel intensity histogram pattern characteristically showed distinct main peak of S-DNA predominantly neoplasm. CAS 200 method was efficient in distinguishing cell cycle phases as S, M peaks.[10] However, more detailed quantitative analysis is required to correlate specific cell populations with image responses, and specific ionic responses with molecular events induced by the chemotherapy.

Proton MRI uses the hydrogen nucleus. It is ideal for structural studies and angiography. The purpose of developing clinical diagnostic approaches using Na-MRI was due to the major involvement of Na in important dynamic processes in the cell, one of which, illustrated here, is interaction of chemotherapy, cellular apoptosis and ions. The ease with which sodium images can be co-registered with proton high resolution images is a further advantage of this technique as is the fact that it does not require costly or potentially toxic reagents as does traditional SQ Na MRI or the new techniques used in gene marker or receptor imaging.

Conclusion

Integrated sodium MRI and PET imaging approach may offer *in vivo* physiological, functional and morphological insights into tumors as a rapid drug monitoring time-dependent method. These tumor imaging (without use of contrast reagents) and cancer cell culture techniques reflected the value of ions (for MRI) and physiological weight (for PET) images with supportive data on cell culture DNA fragmentation, NMR peaks and flow cytometry. The different cell lines cultured demonstrated flow cytometry, fluorescent endlabelling, DNA fragment and NMR data that may be used as a tool for molecular target probes

to evaluate the drug chemosensitive effect. The histoimmunological, ss-DNA staining data was suggestive of apoptosis. NMR peaks were distinct and possibly tumor specific. Increased intracellular sodium and flouro 2-deoxy-glucose utilization in tumors may be associated with apoptosis as a result of accumulation of NMR visible metabolites.

Acknowledgments

This manuscript was in part presented at the peer-reviewed AFLAC Award at the AACR Meeting in 2002, ISMRM Workshop in 2001, and at the ISMRM Annual Meeting in 2002. The authors wish to acknowledge the experimental data and facilities provided by Ed X. Wu, Richard Kline and Kenny Hess at the Radiology department, and Matthias Schbolcs at the Pathology department, and their help in the imaging and continuing tumor histology experiments.

References

1. Evan G, Vousden K, Proliferation, cell cycle and apoptosis in cancer. *Nature* 2001; 411: 342-348.
2. Barbiero G, Duranti F, Bonelli G et al. Intracellular ionic variations in the apoptotic death of L cells by inhibitors of cell cycle progression. *Exp cell Res* 1995; 217: 410-418.
3. Elledge SJ. Cell Cycle Checkpoints: preventing an identity crisis. *Science* 1996; 274:1664-1671.
4. Sharma V, Luker GD, Piwnica-Worms D. Molecular imaging of gene expression and protein function in vivo with PET and SPECT. *J Magn Reson Imaging* 2002; 16:336-351.
5. Gillies RJ, Raghunand N, Karczmar GS. MRI of the tumor microenvironment *J Magn Reson Imaging* 2002; 16:430-450
6. Kurhanewicz J, Swanson MG, Nelson SJ, Vigneron DB. Combined magnetic Resonance Imaging and Spectroscopic Imaging Approach to molecular imaging of prostate cancer. *J Magn Reson Imaging* 2002; 16:451-463.
7. Padhani AR. Dynamic contrast-enhanced MRI in clinical oncology: current status and future directions. *J Magn Reson Imaging* 2002; 16:407-422.
8. Sharma R, Katz J. Minimization of data acquisition in intracellular sodium $[Na]_i$ weighted microimaging using inversion recovery pulse sequence at 4.23 Tesla MRI to correlate increased $[Na]_i$ in apoptosis rich tumors. In Proceedings of ISMRM Workshop on "Data Minimization: More Outcome with less" Marco, Florida, 18-21th Oct. 2001, pp 68-72.
9. Kline R, Wu EX, Petrylak DP, Szabolcs M, Alderson PO, Weisfeldt ML, Cannon PJ, Katz J Rapid in vivo monitoring of chemotherapeutic response using weighted sodium magnetic resonance imaging. *Clin Cancer Res* 2000; 6(6):2146-2156.
10. Sharma R, Katz J. Quantitative Validation of in vivo Intracellular Sodium acquisition at 4.2 T MRI by applying Inversion Recovery Pulse: First Intracellular Sodium-Cell S phase Correlation Analysis. In Proceedings of ENC conference on NMR, Session W&TH P No. 155, Orlando, Florida, 5-16 March, 2001.
11. Sharma R, Esser PD, Van Heertum RL, Katz J. Rapid in vivo monitoring of PC3 induced prostate tumor response to Taxotere in nude mice using PET and H/Na-23 MRI and anti-ss-DNA monoclonal antibody histological characterization. Abstract 10-5039 at 93th Annual Meet of AACR, San Francisco, CA, 2002.
12. Li X, Traganos F, Mclamed M, Darzynkiewicz Z. Single-step procedure for labeling DNA strand breaks with fluorescein- or BODIPY-conjugated deoxynuclleotides: detection of apoptosis and bromodeoxyuridine incorporation. *Cytometry* 1995; 20:172-180.
13. Vermes I, Haanen C, Steffens-Nakken H. Reutelingsperger CPM. A novel assay for apoptosis: flow cytometric detection of phosphatidylserine expression on early apoptotic cells using fluorescein labeled Annexin V. *Immunol Methods* 1995; 184: 39-51.
14. Mochiuzuki T, Tsukamoto E, Kuge Y et al. FDG uptake and glucose transporter subtype expressions in experimental tumor and inflammation methods. *J Nucl Med* 2001; 42:1551-1555.
15. Kubota K, Kubota R, Yamada. FDG accumulation in tumor tissue. *J Nucl Med* 1993; 34:419-421.
16. Hoekstra C, Paglianiti I, Hoekstra O, et al. Monitoring response to therapy in cancer using [18F]-2-fluoro-2-deoxy-D-glucose and positron emission tomography: an overview of different analytical methods. *Eur J Nucl Med* 2000; 27: 731-743.
17. Wahl R, Hutchins G, Buchsbaum D, et al. 18F-2-deoxy-2-fluoro-D-glucose(FDG) uptake into human xenografts: feasibility studies for cancer imaging with PET. *Cancer* 1991; 67: 1544-1550.

18. Krohn K, Mankoff D, Eary J. Imaging cellular proliferation as a measure of response to therapy. *J Clin Pharmacol* 2001; 41: 96S-103S.
19. Woods RP, Mazottia JC, Cherry SR. MRI-PET Registration with automated algorithm *J Comput Assist Tomogr* 1993; 17:4, 536-546.
20. Nishioka T, Shiga T, Shirato H, Tsukamoto E, et al. Image fusion between 18FDG-PET and MRI/CT for radiotherapy planning of oropharyngeal and nasopharyngeal carcinomas. *Int J Radiat Oncol Biol Phys* 2002; 53(4):1051-1057.
21. Golovina VA, Song H, James PF, et al. Na^+ Pump Alpha-2 Subunit Expression Modulates Ca^{2+} Signaling. *Am J Physiol Cell Physiol* 2003; 284:C475-C486.
22. Winslow JL, Cooper RL, Atwood HL. Intracellular ionic concentration by calibration from fluorescence indicator emission spectra, its relationship to the K(d), F(min), F(max) formula, and use with Na-Green for presynaptic sodium. *J Neurosci Methods* 2002; 118(2):163-175.
23. Liebling MS, Gupta RK. A comparison of intracellular sodium ion concentrations in neoplastic and nonneoplastic human tissue using 23Na NMR spectroscopy. *Ann N Y Acad Sci* 1987; 508:149-63.
24. Bednarek A, Shilkaitis A, Green A, et al. Suppression of cell proliferation and telomerase activity in 4-(hydroxyphenyl)retinamide-treated mammary tumors. *Carcinogenesis* 1999; 20(5):879-883
25. Oyama N, Kim J, Jones LA, Mercer NM, et al. MicroPET assessment of androgenic control of glucose and acetate uptake in the rat prostate and a prostate cancer tumor model. *Nucl Med Biol* 2002; 29(8):783-790.
26. Lukacs GL, Zs-Nagy I, Steiber J, et al. Relative intranuclear magnesium and phosphorus contents in normal and tumor cells of the human thyroid gland as revealed by energy-dispersive X-ray microanalysis. *Scanning Microsc* 1996; 10(4):1191-1200.
27. Nagy I, Toth L, Szallasi Z, Lampe I. Energy-dispersive, bulk specimen X-ray microanalytical measurement of the intracellular Na^+/K^+ ratio in human laryngeal tumors. *J Cancer Res Clin Oncol* 1987; 113(2):197-202.
28. Rosini P, Bonaccorsi L, Baldi E, et al. Androgen receptor expression induces FGF2, FGF-binding protein production, and FGF2 release in prostate carcinoma cells: role of FGF2 in growth, survival, and androgen receptor down-modulation. *Prostate* 2002; 53(4):310-321.
29. Mastbergen SC, Duivenvoorden I, Versteegh RT, et al. Cell cycle arrest and clonogenic tumor cell kill by divergent chemotherapeutic drugs. *Anticancer Res* 2000; 20(3A):1833-1838.
30. Rockwell P, O'Connor WJ, King K, et al. Cell-surface perturbations of the epidermal growth factor and vascular endothelial growth factor receptors by phosphorothioate oligodeoxynucleotides. *Proc Natl Acad Sci USA* 1997; 94(12):6523-6528.
31. Kopper KL, Adorante JS. Regulation of intracellular calcium in N1E-115 neuroblastoma cells: the role of Na^+/Ca^{2+} exchange. *Am J Physiol Cell Physiol* 2002; 282(5):C1000-C1008.
32. Lee VM, Quinn PA, Jennings SC, Halligan AW, et al. Altered Na^+/H^+ exchanger isoform 1 activity in immortalized lymphoblasts from women with pre-eclampsia: evidence for an intermediate phenotype. *Clin Sci (Lond)* 2002; 103(5):503-509.
33. Veldhuis WB, van der Stelt M, Delmas F, et al. In vivo excitotoxicity induced by ouabain, a Na^+/K^+-ATPase inhibitor. *J Cereb Blood Flow Metab* 2003; 23(1):62-74.
34. Winter PM, Bansal N. Triple-quantum-filtered (23)Na NMR spectroscopy of subcutaneously implanted 9l gliosarcoma in the rat in the presence of TmDOTP(5-1). *J Magn Reson* 2001; 152(1):70-78.
35. Winter PM, Poptani H, Bansal N. Effects of chemotherapy by 1,3-bis(2-chloroethyl)-1-nitrosourea on single-quantum- and triple-quantum-filtered 23Na and 31P nuclear magnetic resonance of the subcutaneously implanted 9L glioma. *Cancer Res* 2001; 61(5):2002-2007.
36. Hara T, Kosaka N, Kishi H. Development of (18)F-fluoroethylcholine for cancer imaging with PET: synthesis, biochemistry, and prostate cancer imaging. *J Nucl Med* 2002; 43(2):187-199.
37. Lyon RC, Pekar J, Moonen CT, McLaughlin AC. Double-quantum surface-coil NMR studies of sodium and potassium in the rat brain. *Magn Reson Med* 1991; 18(1):80-92.
38. Muscella A, Greco S, Elia MG, Storelli C, Marsigliante S. Angiotensin II stimulation of Na^+/K^+ATPase activity and cell growth by calcium-independent pathway in MCF-7 breast cancer cells. *J Endocrinol* 2002; 173(2):315-323.
39. Katsuragi T, Sato C, Guangyuan L, Honda K. Inositol(1,4,5)trisphosphate signal triggers a

receptor-mediated ATP release. *Biochem Biophys Res Commun* 2002; 293(2):686-690.
40. Pitman AG, Hicks RJ, Binns DS, et al. Performance of sodium iodide based (18)F-fluorodeoxyglucose positron emission tomography in the characterization of indeterminate pulmonary nodules or masses. *Br J Radiol* 2002; 75(890):114-121.
41. Kawano K, Ikari A, Nakano M, Suketa Y. Phosphatidylinositol 3-kinase mediates inhibitory effect of angiotensin II on sodium/glucose cotransporter in renal epithelial cells. *Life Sci* 2002; 71(1):1-13.
42. Nishio M, Ruch SW, Wasserstrom JA. Positive inotropic effects of ouabain in isolated cat ventricular myocytes in sodium-free conditions. *Am J Physiol Heart Circ Physiol* 2002; 283(5):H2045-H2053.
43. Bredella MA, Caputo GR, Steinbach LS. Value of FDG positron emission tomography in conjunction with MR imaging for evaluating therapy response in patients with musculoskeletal sarcomas. AJR *Am J Roentgenol* 2002; 179(5):1145-1150.
44. Hathaway PB, Mankoff DA, Maravilla KR, et al. Value of combined FDG PET and MR imaging in the evaluation of suspected recurrent local-regional breast cancer: preliminary experience. *Radiology* 1999; 210(3):807-814.
45. Kay PA, Riehle DL, Cheville JC, et al. Comparison of quantitative histomorphometry and DNA ploidy in tissue sections of prostate carcinoma. *Anal Quant Cytol Histol* 2002; 24(1):7-14.